RSC Publishing Faraday Discussions

Electroanalysis using modified hierarchical nanoporous carbon materials

Journal:	*Faraday Discussions*
Manuscript ID:	Draft
Article Type:	Paper
Date Submitted by the Author:	n/a
Complete List of Authors:	coneo-rodriguez, rusbel; universidad nacional de rio cuarto, chemistry Baena-Moncada, Angélica; Universidad Nacional de Río Cuarto, ; universidad nacional de rio cuarto, chemistry acevedo, diego; universidad nacional de rio cuarto, chemistry Planes, Gabriel; Universidad Nacinal de Río Cuarto, ; Universidad Nacional de Río Cuarto, Miras, María; Universidad Nacional de Rio Cuarto, Departamento de Química barbero, cesar; universidad nacional de rio cuarto, chemistry

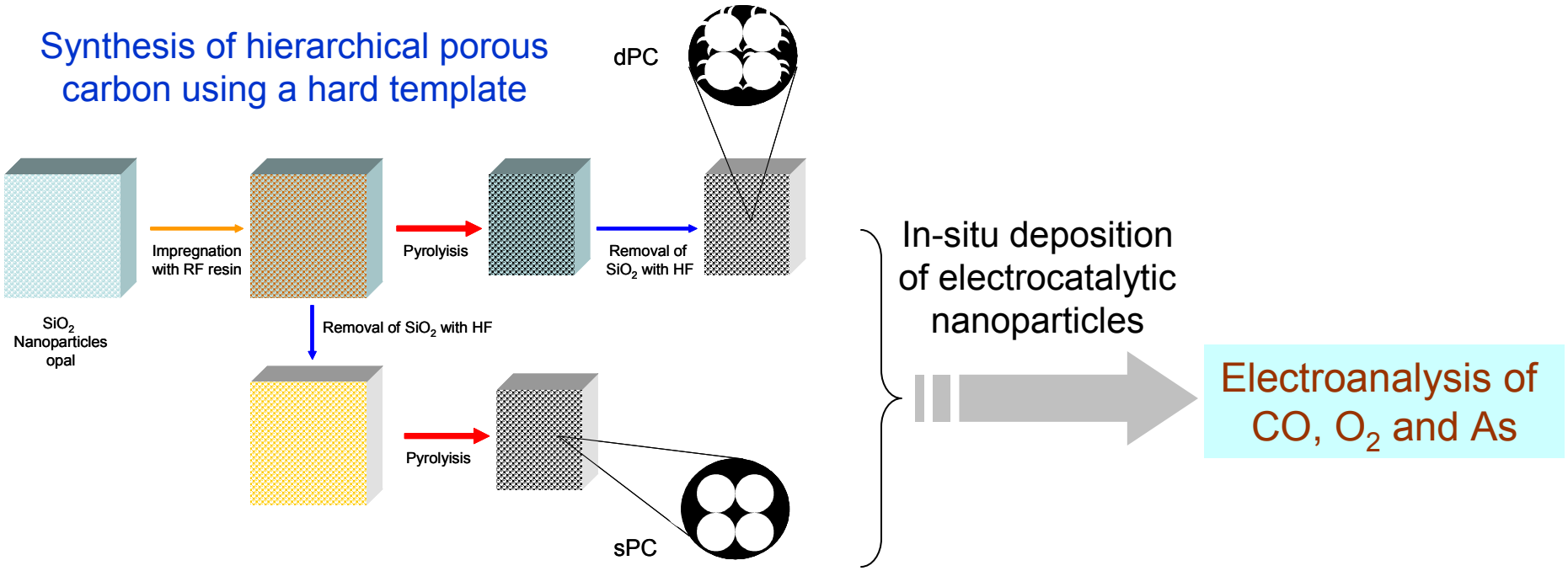

Hierarchical porous carbon (HPC) materials are synthesized using a hard template method. The HPC are modified by in-situ (inside the pores) formation of metal (Pt/Ru), metal oxide (CoOx, Fe_3O_4) or mixed (Pt/ Fe_3O_4) nanoparticles. The modified HPC materials are used for the electroanalysis of different substances (CO, O_2, AsO_3^{-3}). The role of the nanoporous carbon substrate in the electroanalytical data is discussed.

Cite this: DOI: 10.1039/c0xx00000x

www.rsc.org/xxxxxx

ARTICLE TYPE

Electroanalysis using modified hierarchical nanoporous carbon materials

Rusbel Coneo Rodriguez,[a] Angelica Baena Moncada,[a] Diego F. Acevedo,[a] Gabriel A. Planes,[a] Maria C. Miras[a] and Cesar A. Barbero[a*]

Received (in XXX, XXX) Xth XXXXXXXXX 200X, Accepted Xth XXXXXXXXX 200X
DOI: 10.1039/b000000x

The role of the electrode nanoporosity in electroanalytical processes is discussed and specific phenomena (slow double layer charging, local pH effects) which can be present in porous electrode are described. Hierarchical porous carbon (HPC) materials are synthesized using a hard template method. The three dimensional carbon porosity is examined using scanning electron microscopy on flat surfaces cut using a focused ion beam (FIB-SEM). The electrochemical properties of the HPC are measured using cyclic voltammetry, AC impedance, chronoamperometry and Probe Beam Deflection (PBD) techniques. Chronoamperometry measurements of HPC seems to fit a transmission line model. PBD data show evidence of local pH changes inside the pores, during double layer charging. The HPC are modified by in-situ (chemical or electrochemical) formation of metal (Pt/Ru) or metal oxide (CoOx, Fe_3O_4) nanoparticles. Additionally, HPC loaded with Pt decorated magnetite (Fe_3O_4) nanoparticles is produced by galvanic displacement. The modified HPC materials are used for the electroanalysis of different substances (CO, O_2, AsO_3^{-3}). The role of the nanoporous carbon substrate in the electroanalytical data is evaluated.

Introduction

Carbon materials are widely used in electroanalytical chemistry. [1] Among them, glassy carbon (GC) is used as electrode substrate in electroanalytical research, by depositing sensitive materials onto flat GC surfaces.[2,3] Graphite and related materials are the most commonly used component of carbon paste electrodes.[4] Novel forms of carbon, such as carbon nanotubes,[5] and graphene,[6] have been shown to be useful in electrochemical sensing. Besides the low cost and extensive availability of carbon materials, the novel forms allowed to nanostructure the surface, producing materials with novel properties. The main advantage is the creation of large active surface area in small devices.

On the other hand, there are different methods to produce nanoporous GC. Since the chemical and electrochemical properties of GC are well known, it is possible to produce plain GC or modified electrodes with large surface areas. The synthetic methods allow tuning the porosity, creating not only micropores (d< 2 nm) but also mesopores (2 < d < 50 nm) and macropores (d > 50 nm). In that way, not only the surface area but the mass transport of analytes can be controlled.[7]

Using nanoporous microparticles, large surface area electrodes could be built or small microelectrodes with reasonable areas can also be fabricated. A porous carbon (A_{sp}=500 m^2/g) microsphere (r = 10 μm) adsorbed on a 20 μm diameter ultramicroelectrode will have a surface area of ca 0.02 cm^2. Therefore, for a reversible one electron transfer of a redox couple (Co =1 μM), a faradaic current of ca. 0.36 mA (at 100 μs) will be observed. On the other hand, a compact carbon sphere will have a surface area of 1.25 x 10^{-5} cm^2 (at 100 μs). Therefore, the faradaic current will be of ca. 0.2 μA. In this case, the faradaic current increases 1800 times by using the porous material, while maintaining the same geometrical area of the electrode.

We have extensively studied the synthesis of porous carbons by pyrolysis of porous polymeric (resorcinol/formaldehyde) resins (RF).[8,9] The resin gels maintain its nanoporosity during conventional drying trough stabilization of resin nanoparticles by cationic supramolecular species. The carbon source (precursor) is subjected to a heat treatment (pyrolysis) at high temperature in the absence of oxygen to produce the carbon.

Porous carbon can be obtained using templates of nanometric sizes.[10,11] Since precursor materials are organic polymers, containing hydrogen and oxygen besides carbon, the pyrolysis involve mass loss and volume contraction. Soft templates like polymers and surfactants are spontaneously eliminated during burning of the carbon material, therefore post treatments are not necessary. On the other hand, hard templates like silica and metal oxides survive to high temperatures, and must be removed after pyrolysis by chemical etching. In this process, the space initially occupied by the templates is transformed into the pores in the resulting carbon materials. The whole process result in a reverse copy of the template.[12]

We have shown that the micrometric fibers also stabilize the nanopores during drying.[13] In that way, a spontaneous hierarchical carbon material (bearing macropores and mesopores) could be produced. Since the main research goal was to produce electrode materials for supercapacitors,[14] both capacitance and response rate should be maximized.

While capacitance depends mainly on the surface area, the response rate is related with the mass transfer and/or potential effects inside the pores, which depends on the length and tortuosity of the pores. One way to overcome such problems involves the fabrication of hierarchical porous carbons, having both macropores and meso/micropores. The presence of macropores makes the length of the meso/micropores small (< 10

μm) and could make the mass transfer fast enough. [15]

Hierarchical porous carbon,[16,17,18] can be obtained using two templates in a somewhat complex processes. On the other hand, we have recently shown that the volume contraction of the carbon, around a remaining hard template, during pyrolysis induces the formation of additional mesoporosity, besides the pores defined by the hard template, is able to create a hierarchical carbon material.[19] In that way, hierarchical porous carbon can be obtained in a single pyrolysis step.

Porous materials (e.g. carbon) are usually characterized by measuring the adsorption isotherm of inert gases (e.g. N_2). Modelling the adsorption data, the surface area, pore volume and pore size distribution can be evaluated. However, in electrochemical applications only the surface area accessible to the electrolyte is important. It is well known that small micropores cannot be filled with electrolyte and do not contribute to the electrochemical active area but are measured by the gas adsorption isotherms.[20] Therefore, in-situ measurements of ion adsorption phenomena such as differential capacitance,[21] or Probe Beam Deflection (PBD),[22] render more useful data of the carbon texture. PBD has shown to be very useful to study porous materials,[23,24] including carbon aerogels.[25] The application of the technique allows to distinguish between systems with fast mass transfer (where all the charging/discharging phenomena occurs in a negligible time, called discontinuous process) and slow mass transfer (where the charging/discharging phenomena occurs during the whole measurement). Such distinction is quite important for the electroanalytical application of the materials.

In the present work, we used the technique to study the changes on ion concentration occurring inside the pores when the state of charge of the carbon materials is altered. An important point here is that, unlike planar electrodes, porous electrodes could develop local ion concentration gradients inside the pores (e.g. H^+) which are different from bulk values. Those local phenomena could heavily affect the electrocatalytic activity.

On the other hand, a direct way to measure textural properties of disordered porous carbon is still missing. We have used a nanotomography method based on the cutting of thin slices of the porous material using a focused ion beam (FIB) of Ga ions. Then, microscopic images of the exposed surfaces are taken with a field emission scanning electronic microscope (FE-SEM). The images are reconstructed onto a 3D image of the solid.[26] The slices (z axis) can be as thin as 10 nm and the resolution of the FE-SEM is ca. 1 nm. We have used the technique to study porous carbon materials.[27] In the present work, we used it to study the macroporosity of hierarchical porous carbon.

Metal nanoparticles have been extensively used as electrocatalysts in fuel cells research, and have potential use in electroanalysis.[28] PtRu catalysts are the most active for methanol oxidation,[29] likely due to the formation of Ru oxides in the surface which are able to oxidize adsorbed poisons like CO. Such behaviour would allow to oxidize other organic species of analytical interest (e.g. glucose[30]) which does not present reversible redox couples but have oxygenated groups or C-H bonds which can be irreversibly oxidized. Different electrode systems, such as electrochemical deposited Ru on Pt, bulk PtRu alloys and electrodeposited PtRu alloys, have been studied.[31,32,33] We have investigated the electrooxidation of methanol at mesoporous (MP) Pt and Pt–Ru electrodes.[34] Pure metal mesoporous catalysts (mesoporous Pt modified by adsorbed Ru) show improved surface activities, with values as high as 0.82 A cm^{-2} However, differential electrochemical mass spectrometry (DEMS) measurements with pure metal catalysts reveal that only a half of the current obtained during methanol electrooxidation produce CO_2 while in commercial catalysts (20 % Pt/Ru 1:1 on carbon, E-TEK®) all the current produces CO_2 (conversion efficiency ca. 100 %). It is likely that such differences in catalytic activity towards methanol oxidation are due to diffusion effects taking place in the catalytic film. In the present work we show the successful deposition of PtRu inside hierarchical porous carbon (dPC), by a chemical method and the application of the electrode (PtRu-dPC) to detect carbon monoxide and methanol.

Redox metal oxides are widely used in electrocatalysis.[35,36] Therefore, they have also been used in electroanalysis. [37] Cobalt oxide nanoparticles (CoOxNP) could be easily deposited electrochemically onto flat GC electrodes.[38] They have been used for determination of hydrogen peroxide,[39] and arsenic ions. [40] In the present work we show the successful deposition inside hierarchical porous carbon (CoOxNP-dPC) and its use to detect arsenic ions and oxygen.

Additionally, we shown that it is possible to deposit magnetite (Fe_3O_4) nanoparticles (MagNP) inside hierarchical porous carbon, by a well known chemical method,[41] to produce an electrocatalytic electrode material (MagNP-dPC). This material is used to detect arsenite ions using differential pulse voltammetry. By galvanic displacement,[42] the supported magnetite nanoparticles are decorated with Pt (PtMagNP-dPC). The electrode is able to reduce oxygen in the presence of a large concentrations of methanol.

In summary, we use different examples of the current work in our group to discuss some points which we feel are important in the use of nanoporous electrode materials in electroanalysis:

- that large electrochemically active areas could improve the signal/noise ratio of electroanalytical measurement, but the length of the pores should be kept at minimum to be able to discern the faradaic current from the slow double layer charging.
- that hierarchical carbon systems are interesting materials for electroanalytical applications since they possess both large surface areas and good accessibility of solution analytes to the electrode surface.
- that direct characterization techniques of the carbon porous structure are necessary the understand the role of the electrode material in the electroanalytical responses.
- that local pH gradients could easily develop inside the pores, in neutral solution, due simply to double layer charging coupled with slow mass transfer. Such pH changes could affect the electrocatalysis and/or chemistry coupled to the electrochemical reaction.
- that the modification of porous carbon with metal or metal oxide nanoparticles, a method extensively explored in fuel cell research, could be used with profit in electroanalysis.

Experimental

All reagents are of analytical grade and Millipore® quality water is used.

Materials

Synthesis of the hierarchical porous carbon

Hierachical porous carbon is synthesized by a hard template approach, using SiO_2 nanospheres as moulding agent (Scheme 1). The SiO_2 nanoparticles (SiO_2-NP) of different diameters (typical 400 nm) were synthesized by the Stober method, that is TEOS hydrolysis in basic media.[43] The diameter of SiO_2-NP were determined by dynamic light scattering (DLS, Malvern 4700 with goniometer and 7132 correlator) with an argon-ion laser operating at 488 nm. All measurements were made at the scattering angle of 90º. The nanoparticle dispersity (measured by dynamic light scattering) is quite low. The SiO_2-NP were then deposited by gravitational sedimentation in the bottom of a vial.[17]

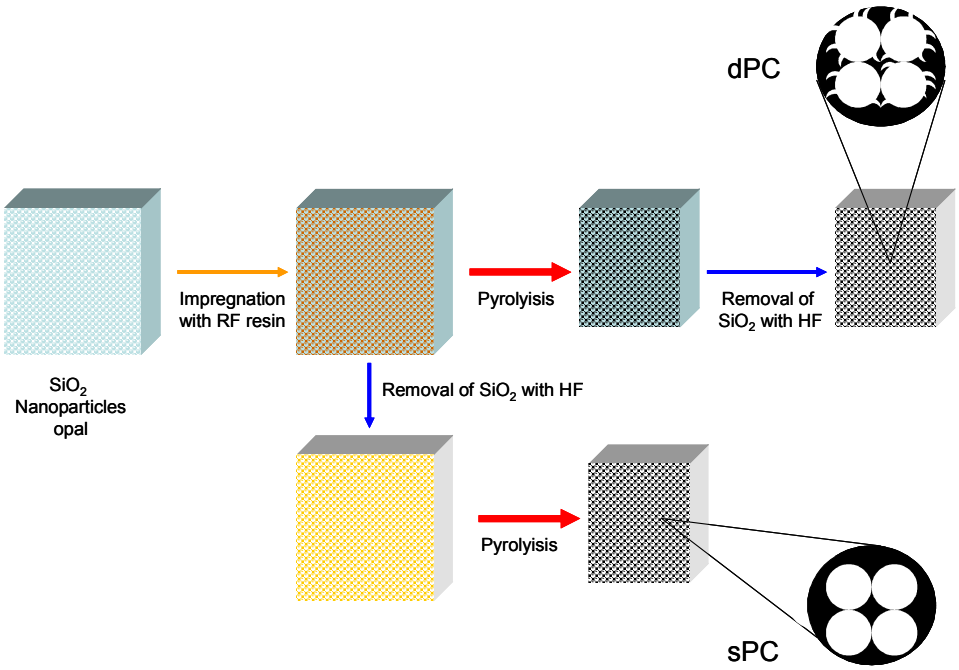

Scheme 1

Synthetic method to produce double pore carbon (dPC) or single pore carbon (sPC) using SiO_2 nanoparticles as hard template of resorcinol/formaldehyde resin.

After solvent evaporation, the resulting opal was taken out of the vial and then treated at 1000 ºC for 4 hours to form a connected matrix of SiO_2 nanospheres (ESI Figure S1). While there is no long range order in the opal, it is clear that could be used as sacrificial template for a different solid which could be synthesized inside the interstitial space between spheres. In our case, the opal was impregnated with a carbon precursor, a mixture of resorcinol (1 g), formaldehyde (1.6 ml), and sodium carbonate (catalyst, 0.4 ml of 0.1 M solution). The impregnated SiO_2 opal was dried in an oven and heated at (105 ºC) in air during 12 hs to polymerize the resorcinol/formaldehyde mixture and obtain an opal impregnated resin (SiO_2-RF). To obtain the final carbon the RF resin should be carbonized by heating in inert atmosphere.[44] Based on previous data,[19] two methods of post-processing could be used: i) the SiO_2 is removed before pyrolysis by treatment with hydrofluoric acid solution (Single Pore Carbon, sPC). ii) The composite (SiO_2-RF) is pyrolyzed and the SiO_2 removed afterwards by treatment with hydrofluoric acid solution (Double Pore Carbon, dPC). The pyrolysis of both samples was carried out at 850 ºC for a 24 h. The corresponding morphological characterizations were performed by means of SEM, HRTEM and FIB-SEM.

Deposition of PtRu nanoparticles inside porous carbon (PtRuNP-sPC)

The carbon **(s**PC**)** was loaded (20 % metal) with Pt/Ru nanoparticles using a variation of the formic acid method.[45] Due to the nature of the material to be impregnated, a porous solid with particle size around 25 µm, the order in which reactants are added to the carbon suspension was modified. In the conventional method, the last step involves the addition of the metallic precursors to be reduced. However for the porous carbon microparticles, the metallic precursors must reach the nanoparticle cores before the reduction starts. For this reason, the first step here is the addition, under vigorous stirring, of metal precursors to the HPC. This mixture is keeping under stirring for 12 h, then the process is completed by the addition of an excess of formate solution (preceded by pH adjusting to 10). Finally, the PtRu-sPC is washed with copious quantities of water, filtered and dried for its storage.

Deposition of cobalt oxide nanoparticles inside porous carbon (CoOxNP-dPC)

Cobalt oxide nanoparticles were deposited electrochemically as described before.[37] A GC electrode modified by a porous carbon layer was cycled (50 mVs^{-1}, between -1.1 V and 1.25 $V_{Ag/AgCl}$) in a solution containing 0.01 M $CoCl_2$ and 0.1 M CH_3COONa. In the buffered solution, the Co^{II} ions are soluble but the Co^{III} species form an insoluble deposit. The amount of material was controlled by the number of deposition cycles (15 to 30 cycles).

HPC carbon loaded with magnetite (Fe_3O_4) nanoparticles (MagNP-dPC).

To synthesize in-situ magnetite (Fe_3O_4) nanoparticles inside the porous carbon, we used a procedure described before for the synthesis of free nanoparticles.[46] Powdered porous carbon (100 mg) is mixed with 25 ml of a solution consisting of 0.2 M ferric chloride ($FeCl_3.6H_2O$) and 0.1 M ferrous chloride ($FeCl_2.6H_2O$). The Fe/C ratio used is ca. 20% w/w. The mixture si subjected to magnetic stirring during 20 hs, to incorporate the solution inside the carbon. After that, 25 ml of NaOH solution (0.1 M) are added dropwise. A black precipitate is formed instantaneously. The excess reactants are washed out with distilled water while the magnetite containing material is holded at the bottom of the tube with a magnet.

Synthesis of Pt/magnetite nanoparticles on HPC (PtMagNP-dPC)

The Pt/magnetite nanoparticles were synthesized by galvanic displacement method,[47] using magnetite nanoparticles as sacrificial material. Carbon loaded with magnetite nanoparticles synthetized as described above, was mixed with hexachloroplatinic acid solution (0.01 M). The presence of Pt was detected by the presence of hydrogen reduction current (in acid media) below 0.1 V_{RHE}.

Deposition of porous carbon particles on GC

A carbon ink is prepared by dispersing the powdered material in a solution Nafion®/water/ethanol. The ink was prepared by dispersing 4 mg of carbon in 1ml of distilled water with 15 µl of 10 % solution Nafion® in ethanol. The mixture was dipersed using ultrasound. To prepare the deposit, 10 ml of the ink were placed onto a flat GC surface and the solvent was evaporated in still air.

Methods

Scanning electron microscopies

Carbon morphology was observed using a field emission scanning electron microscope. A dual beam workstation (FEI Helios Nanolab 600) equipped with a FIB column employing a gallium liquid metal ion source, combined with a field emission gun scanning electron microscope (SEM) was used. The SEM column was used for general imaging and the FIB column was used for cross-section preparation.[48]

Electrochemical characterization of the HPC support.

The electrochemical performance of the carbon electrodes was analyzed with a three electrode configuration. N_2 was bubbled through the solution to avoid dissolved oxygen. The working electrodes are glassy carbon rods (3 mm diameter) inserted in teflon, where a carbon ink was deposited (see below). A carbon aerogel (Maketech, geometrical area 5 times of the working electrode) and a silver/silver chloride electrode (saturated KCl) were used as counter and reference electrode. Cyclic voltammetry (CV) and the AC impedance measurements were performed using a PC4 Potentiostat-Galvanostat-ZRA (Gamry Instruments, Inc).

Cyclic voltammetry

Cyclic voltammetry was carried out to test the electrochemical active area of both samples. An electrochemical evaluation of the carbon area has been preferred here due our interest in using these materials as supporting materials for fuel cell catalysts,[49] but can be usefull also in other electrochemical devices for energy production and storage,[17] like electrochemical double layer capacitors,[50,51] and carbon/graphite composed materials for Li ion batteries.[52,53] This measurement gives an accurate idea of the accessible surface for any electrochemical process in aqueous media. The differential capacitance was calculated as:

$$Cd = \frac{dQ}{dE} = \frac{dQ}{dt}\,\frac{dt}{dE} = i\,v \qquad (1)$$

where Q is the charge, E de potential, t the time, i is the current and *v* the scan rate.

Using the current in amperes and the scan rate in volts per second, the differential capacitance is obtained in farads. Assuming that the capacitance surface density is constant, the capacitance gives a comparative idea of the extension of the electroactive area. However, it is known that surface redox groups (quinone like) could contribute to the capacitance value. Since these groups are active in acid media, the capacitance is measured in neutral media. The current in the resulting cyclic voltammograms was divided by the scan rate and the electrode mass to obtain specific capacitance vs. voltage profiles.

AC impedance

The AC impedance measurements were performed using a computerized potentiostat (GAMRY PC4) and CM 300 impedance software. The cell configuration has three electrodes with a counter electrode of carbon aerogel (Maketech, geometrical area 5 times of the working electrode) situated parallel to the working electrode and a reference electrode of SCE. The carbon aerogel was used as counter electrode to assure that its electrochemical active area was bigger than that of the working electrode.The measurements were made with a sinusoidal voltage perturbation of 1 mV and a resting time at each potential of 30 min. The circuit simulation and fitting were made using the analysis software in Excel (Microsoft) provided with the equipment.

Probe Beam Deflection

Probe Beam Deflection is a technique that measures the concentration gradient in front of the electrode by monitoring the refractive index gradient with a light beam.[22] The electrochemical charging of the double layer could be accompanied by a ion fluxes due to diffusion and migration. In a binary electrolyte both modes of mass transfer are necessarily coupled and a single binary diffusion coefficient describes the flux. The ion concentration in the solution changes, creating a gradient of refractive index normal to the electrode surface. A beam traveling parallel to the surface suffers a deviation

proportional to the concentration gradient, therefore proportional to the extent and direction of ion flux. Positive beam deflection (away from the electrode) corresponds to incorporation of ions into the double layer while negative deflection (towards the electrode) implies release of ions to the solution. The Probe Beam Deflection arrangement was similar to the one described before.[54] The basic components of the PBD system are a 5 mW He-Ne laser (Melles Griot, 05 LHP11) and a bicell position sensitive detector (UDT PIN SPOT/2D). The laser beam is focused by a 50 mm lens to a diameter of roughly 60 μm in front of the planar electrode. The electrochemical cell, an optical glass cuvette with 2 x 2 x 4 cm dimensions (1 cm of path length), is mounted on a 3 axis tilt table (Newport). A micrometric translation stage allows for controlled positioning of the sample with respect to the laser beam in 10 μm steps. The position sensitive detector is placed 25 cm behind the electrochemical cell and has a sensitivity of 3 mV/1 μm, which resulted in a deflection sensitivity of 1 mrad/V. All parts of the system are fixed on an optical rail and the whole set-up is mounted on an optic table (Melles Griot). The deflection signal was processed using a position monitor (UDT 201 DIV). Due to the fact that PBD signal have to be monitored at long times (> 50 s), the whole system was warmed up for 24 hs before each measurement to eliminate thermal fluctuations. The signal of the two photodiodes making the bicell detector were subtracted and normalized to the overall signal to eliminate laser intensity fluctuations. The chronodeflectometric pulses were fitted using the nonlinear fitting routine of Origin 7.0 (MicroCal). The glass cell contains a counter electrode of aerogel (with geometrical area 5 times the working electrode) and a Ag/AgCl (3 M NaCl) miniature reference electrode (BAS) separated from the solution with a Vycor diaphragm. The working electrodes were carbon composites plates (width 2 mm) attached onto Teflon plates with sides and back sealed and the active side unpolished. The electrochemical control of Probe Beam Deflection experiments was performed using a potentiostat (AMEL 2049). The set-up was controlled by a PC through a LabPC AD/DA card running in homemade software performed with LabView 5.1 (National Instruments). The deflection and the electrochemical signals were saved jointly in the PC.

Electronalytical measurements

Carbon monoxide oxidation

Electrochemical measurements were performed in 1M CH_3OH/1 M H_2SO_4 at 60 ºC, with a PC controlled Autolab PGSTAT30 potentiostat–galvanostat and a thermostatized three electrodes electrochemical cell. We use a hydrogen reference electrode (RHE) in the electrolyte solution as the reference

Oxygen reduction

Oxygen reduction mesaurement were performed in O_2 saturated electrolyte produced by gently bubbling ultrapure (99.99) O_2 gas trough the solution by 15 min.

Arsenic ion oxidation

A mother solution of arsenic ions is prepared by dissolving weighted amounts of arsenic oxide (Aldrich, 99.9%) in 0.1 M NaOH solution. An aliquot of the mother solution is then mixed with phosphate buffer solution (pH=7).

Results and discusion

Theory and numerical calculations

High surface area materials should be useful in electroanalysis because the faradaic signal scale with the active area. However, since the background signal in electrochemical measurement is due to double layer capacitance of the base electrode, its magnitude also scales with the active area. Moreover, small pores (such as micropores d < 2 nm) will contribute to double layer capacitance but are less accessible to mass transfer of analytes from solution. A usual method to eliminate capacitive background signal is to use pulses as perturbation signal. For a planar small electrode, the capacitive charge (related to the background signal) decays exponentially with time while the faradaic charge (related to the analyte signal) decays with the square root of time. Therefore, after a perturbation pulse, the background signal will decay faster than the analytical signal. In that way, measuring at longer times increases the signal/background ratio. Such approach is the basis of pulse voltammetries (normal and differential) and square wave voltammetry.[55] In differential pulse voltammetry (DPV), a small amplitude (10 to 100 mV) potential pulse is superimposed on a slowly changing base potential. Current is measured at two points for each pulse, the first point just before the application of the pulse and the second at the end of the pulse. These sampling points are selected to allow the decay of the nonfaradaic (charging) current. The difference between current measurements at these points for each pulse is determined and plotted against the base potential.[56]

However, the larger electrode area will increase not only the faradaic current but also the charging current, which is related the double layer capacitance. The charging current $i_{cap}(t)$ follow the expression

$$i_{cap}(t) = \frac{\Delta E}{Rs} e^{\left(-\frac{t}{Rs\ Cd_{sp}\ A}\right)} \qquad (2)$$

where ΔE is the potential pulse width, Rs is the cell resistance, A is the electrode area and Cd_{sp} is the aerial capacitance density.

On the other hand, for a simple reversible redox, at a potential where all reactant is converted at the electrode surface, the current will follow Cottrell's equation:

$$i_{far}(t) = nFACo\sqrt{\frac{Do}{\pi t}} \qquad (3)$$

where n is the number of electron exchanged, F is Faraday constant, A is the area and Do is the diffusion coefficient of the redox species.

Using eq. 2 and 3, it is possible to calculate the current dependence con time (Figure 1).

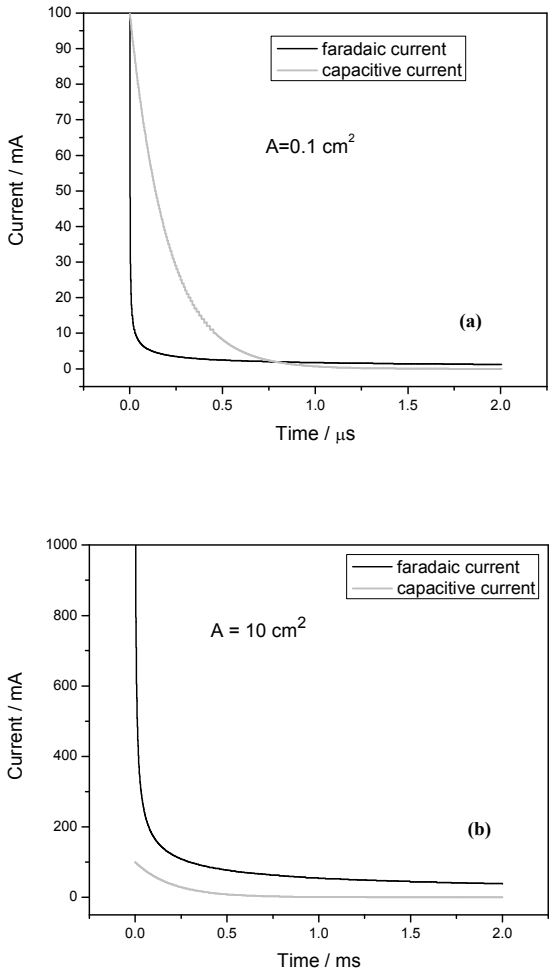

Fig. 1 Calculated capacitive and faradaic current measured after a potential pulse is applied to the electrode.

ΔE = 0.1 V; Cd_{sp}= 20 μFcm^{-2}, Do= 1 10^{-5} cm^{2}s^{-1}, Co=1 10^{-6} M, n=1. (a) A = 0.1 cm^2, (b) A = 10 cm^2.

As it can be seen, for small electrodes (A= 0.01 cm^2, Figure 1.a) the capacitive current is larger than the faradaic current, at small times. At longer times, the faradaic current is larger than the capacitive current. Therefore, the approach of DPV is justified. The question is about large electrodes. For large electrodes (A=10 cm^2, Figure 1.b) the faradaic current is always larger than the capacitive current. It should be bear in mind that it is possible to fabricate an electrode with large active area and small geometrical area (< 1 mm^2) depositing a porous carbon layer on a small flat GC electrode. Using only 1 mg porous carbon (specific area 500 m^{2}g^{-1}), it is possible to produce an electrode with ca. 500 cm^2 of active area. Such electrode will show higher faradaic than capacitive currents at all times. Additionally, there is no need to wait until the double layer charging has decreased to a low value (as it is the case with small electrodes), only the width of the pulse should be kept constant.

The discussion above assume that a porous electrode is only a planar electrode of extended area. However, it was suggested, based on PBD data, that ion transport in monolithic porous carbon occur in a continuous process where the response scale with $\sqrt{t}$.[23] It can be thought that ions have to move inside the pores to compensate the charge inside the porous matrix. If the pores are tortuous and/or of small section, a small diffusion (D < 10^{-7} cm^{2}s^{-1}) through a relatively thick layer (> 200 μm) will mean that 2000 s are necessary to charge the electrode. by pure electrochemical measurements as both predict a dependence of the fluxes with $\sqrt{t}$. To maintain electroneutrality, charge transport is linked to ion transport. It seems paradoxical for double layer charging to be controlled by mass transport, but that is the case in porous materials. Therefore, the current is controlled by the slow ion transport.

An alternative mechanism involve the existence of a transmission line phenomena to account for electric potential profiles inside the pore.[57] In this case, the time profile of the charging current is given by eqn. 4.[58]

$$i(t) = \Delta E \sqrt{\frac{Cd_{sp}\ A}{R_{pore}\pi t}} \left[1 + 2\sum_{n=1}^{\infty} (-1)^{n+1} e^{(-n^2\tau/t)} \right] \qquad (4)$$

where ΔE is the potential step, Rp is the ionic resistance, Cd_{sp} is the specific double layer capacitance and

$$\tau = R_{pore} C_{sp} A = \rho \left(\frac{L}{A S_{pore}} \right) Cd_{sp} A \qquad (5)$$

where ρ is the resistivity, L is the electrode thickness and S_{pore} is the section of the pore.

If $L \to \infty \Rightarrow \tau >> t$, therefore the term between brackets tends to 1, and the current obeys eq. 6:

$$i(t) = \Delta E \sqrt{\frac{Cd_{sp}\ A}{R_{pore}\pi t}} \qquad (6)$$

which defines a semi-infinite transmission line.

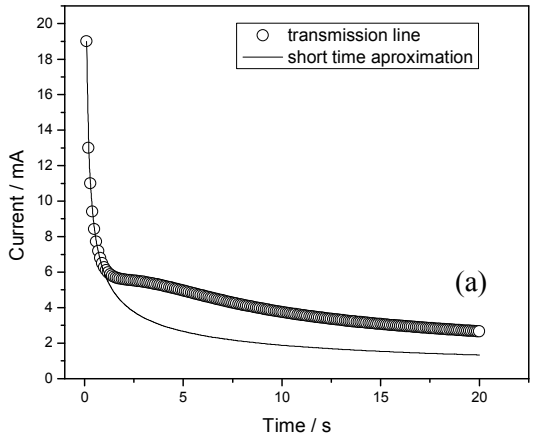

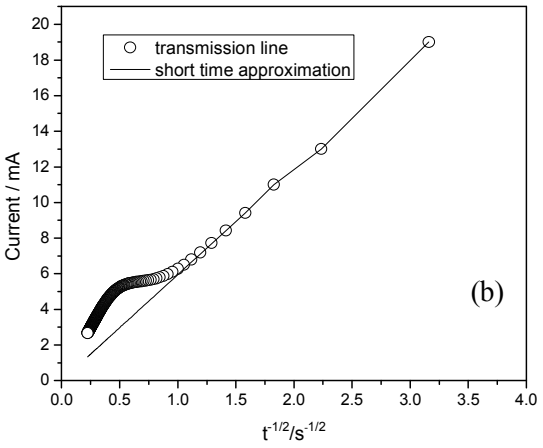

Fig. 2 Simulated time profile of capacitive current for a porous electrode following the full transmission line expression (eq.3, open circles) or the short time approximation (eq.4, full line). (A) current-time profile. (B) Cottrell plot. R_{pore}= 18 ohms. Cd_{sp}= 20 μFcm^{-2}, A=100 cm^2.

As it can be seen in Figure 3, for small concentrations the faradaic current will be smaller than the capacitive current.

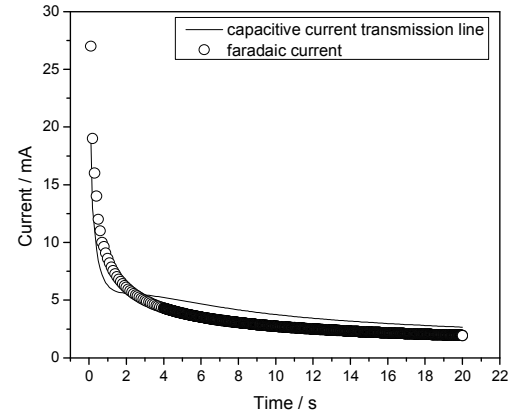

Fig. 3 Simulated responses of the capacitive current (eq.3, full line) and faradaic current (eq. 2, open circles) of a porous electrode. The capacitive current follows the full transmission line expression with Rpore= 18 ohms, Cd_{sp}= 20 μF/cm^2, A=100 cm^2. The faradaic current follows Cottrell equation with Do=1 10^{-5} cm^2/s, Co= 5 10^{-9} M, n=1, A=100 cm^2

The slow charging behaviour precludes, or at least complicates the interpretation, of pulse potential data (including DPV), at least for small concentration of redox species where faradaic current is small. Therefore, experimental conditions should be set to assure that capacitive charging has subsided before the current measurement is taken. This is possible using short mesopores, as those present in hierarchical carbons where the macropores limit the length of the solid mesopores.

On the other hand, in amperometric sensors usually large time pulses (>10 s) are used to allow "stationary" mass transport of the analytes and effective mass transfer of analytes at low concentrations. In such experimental conditions, the decay of the capacitive current is probably complete and only the faradaic current is measured. Obviously, if the mass transfer inside the pores allows the most of the pore area to be electrochemically active, the large electrode area will render a large current signal and improved sensitivity to low concentration of analytes. However, it should be bear in mind that a commonly used technique to test the electrode activity, cyclic voltammetry, at usual scan rates (>10 mVs^{-1}) will be affected by charging current and shows a completely different picture of the system under study.

It should be mentioned that another technique useful to study porous electrodes is Probe Beam Deflection.[22] In this technique two extreme conditions of the double layer charging can be easily detected experimentally:

- *Discontinuous process*: where all the charge (and ions) are stored/released in a time span much samller than the measurement. This condition is related with a RC circuit.
- *Continuous process*: where charge (and ions) are stored/released along the whole measurement. This condition is related with a semi-infinite transmission line.

The condition of a finite transmission line is more complex and have not been yet theoretically analyzed. Each kind of process show a distinctive chronodeflectometric profile, making PBD a usefull technique for porous electrode investigation.

The discussion suggests that hierarchical porous carbon should be a material of interest for electroanalytical applications possessing large surface areas and relatively fast double layer charging. Since carbon is a poor electrocatalyst for the electrochemical reaction of different substances, the carbon surface should be modified by incorporation of electrocatalysts. Porous carbon provides a large surface to adsorb electrocatalytic particles and also could protect the material from erosion by hiding the nanoparticles inside the pores. However, the particles must be of nanometric size to be able to decorate the inner pore surface and not only deposited in the outer surface.

Synthesis of the hierarchical porous carbon

To produce carbon with and open structure, we used silica nanoparticles as hard template. The volume contraction during pyrolysis of RF resin is easily observable by comparison between the piece size before and after thermal decomposition of the precursor. However, when the carbon sample contains a rigid template, the observed contraction in the macroscale is very low due to the presence of a non compressible skeleton. In our case, this rigid support is composed by an array of nanometric SiO_2 nanoparticles in close contact between them. The SEM image of these SiO_2 nanoparticles (ESI. Figure S1) reveals the existence of almost monodisperse spheres with diameter of ca. 390 nm. The observed size agree with the results of the DLS experiments which report a SiO_2 NP diameter around 400 nm, with a polidispersity index of ~3 %. Such low dispersion favours the packing of the nanoparticles into a close packed structure. As it is shown in Scheme 1, the hard template can be eliminated before or after pyrolysis. We have shown,[19] that elimination before pyrolysis produces a carbon with one pore size (sPC) which is directly determined by the template nanoparticle size but takes into account the 20-30 % contraction of the material upon pyrolysis. On the other

hand, if the hard template is left during pyrolysis, the contraction of the solid material has to take place in the interstitial spaces between particles. In that way, the solid becomes microfractured and the carbon has two pore sizes (dPC), one directly related to the hard template size (e.g. 400 nm) and another much smaller in the order of mesopores (< 50 nm). Additionally, the carbon presents the sintered beads of carbon linked into a matrix through necks, which has been proposed as the building block of RF resin. Those beads, after precipitation, form the condensed monoliths.[59,60] Such structure is clearly observed in the fracture (Figure 4.a) cut of a dPC piece. On the other hand, in the flat FIB cut it is possible to observe the open three dimensional nature of the carbon (Figure 4.b).

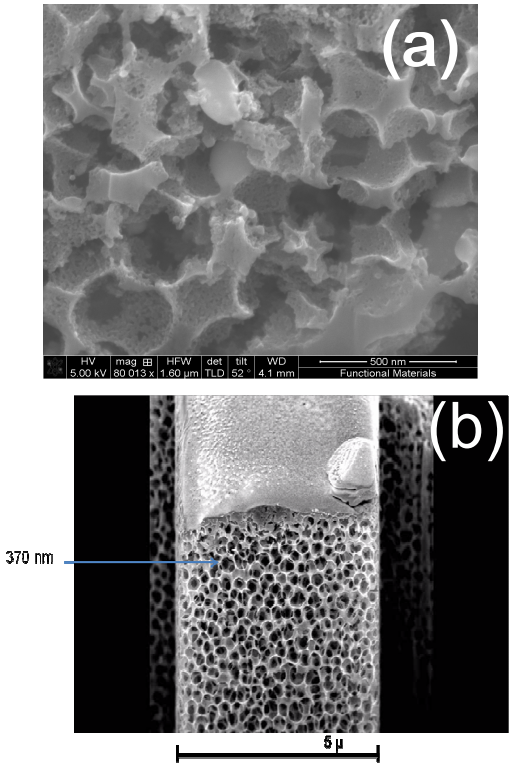

Fig. 4 FE-SEM micrographies of dPC synthesized using an opal of SiO_2 nanoparticles (400 nm diameter) as hard template.(a) Fracture surface. (b) Flat cut made using a FIB (Focused Ion Beam) of Ga.

The macropore structure seems quite open allowing the analyte to easily diffuse to the electrode surface.

Electrochemical characterization of the HPC support

Measurements of double layer capacitances give a semiquantitative value of the extension of the electroactive area and it is quite important to asses the relative contribution of faradaic and capacitive signal. The electrodes made with dPC, where the silica template was removed after pyrolysis, show a CV curve with large differential capacitance (130 F/g of carbon), associated with a large surface area (Figure 5).

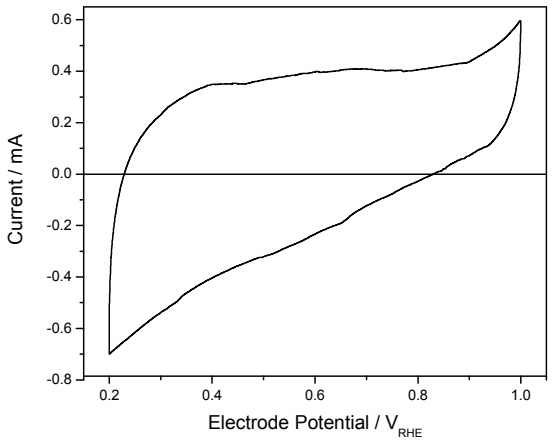

Fig. 5 Cyclic voltammetry of porous carbon (400 nm diameter) in H_2SO_4 1 M. Scan rate = 5 mV s^{-1}. Specific capacitance = 132 Fg^{-1}

This capacitance value is quite similar to that reported before for the other porous carbon.[61] From these values, a specific surface electroactive area of ca. 650 m^2g^{-1} can be roughly estimated (based on a specific capacitance of 20 μFcm^{-2}).[62] The value larger than one expected for the exposed area of the holes left by 400 nm template nanoparticles. Therefore, the contraction of the carbon should have produced nanopores (meso and micropores) in the macropore inner surfaces.

In the case of a carbon material with only one pore size(sPC), where the template of SiO_2 nanoparticles template is removed before pyrolysis (sPC), the cyclic voltammogram (not shown) shows specific capacitance values reduced to ca. 30 Fg^{-1}. Such values correspond to specific surface areas in the order of 150 m^2g^{-1}.

Chronoamperometry

As it was discussed before, the chronoamperometric signal of a porous carbon will follow a transmission line model, which tends to $1/\sqrt{t}$ at short time span (semi-infinite condition). A plot of current as a function of $1/\sqrt{t}$ should be linear (Cottrell plot).

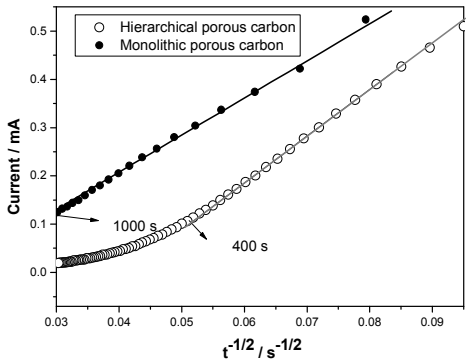

Fig. 6 Cottrell plots obtained by applying a potential pulse (between 0.0 and 0.35 Vsce) to a monolithic porous carbon electrode (full squares) and a hierarchical porous carbon electrode (open circles). Both chronoamperometric data were obtained in 1 M H_2SO_4. The full lines are LSQ linear fits of the linear region of each plot.

This is the case with thick (250 µm) monolithic porous carbon (Figure 6. full squares), indicating that in a long time span (1000 s) the current is controlled by ion transport. On the other hand, for HPC (Figure 6, open circles) the linearity only occur up to 400 s. After that, the full transmission line regime is operative (as shown in Figure 2).

AC Impedance

While chronoamperometry gives a fairly reasonable account of the HPC electrode, it involves large potential excursion. On the other hand, AC impedance uses a small potential amplitude assuring that the measurement is made on a linear system. [63] A typical Nyquist plot of an HPC is shown in Figure 7.a

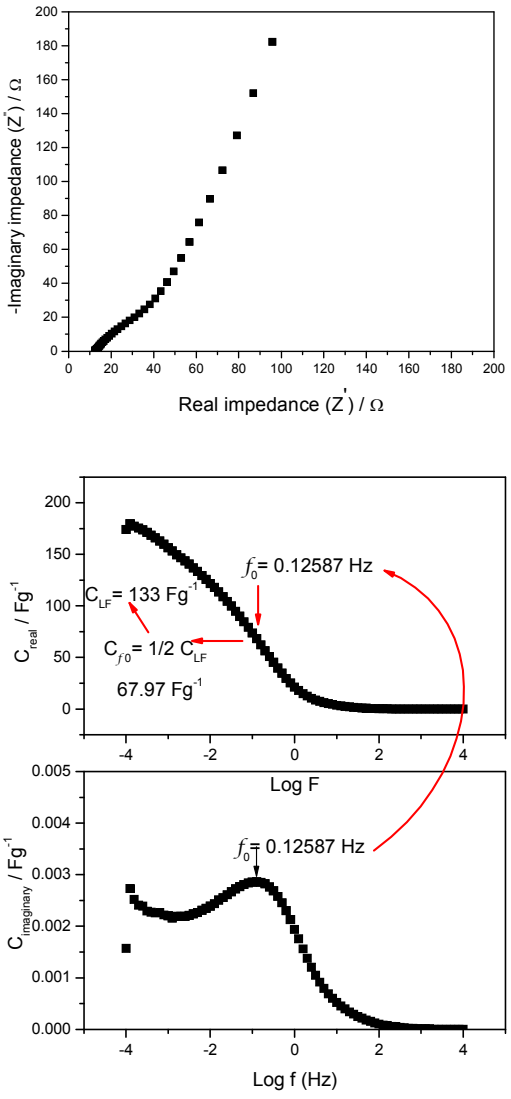

Fig. 7. Impedance dependence with frequency. (a) Nyquist plot (of a hierarchical porous carbon (400 nm) between 0.1 mHz and 10 kHz at 0.65 V_{HRE} in 1 M H_2SO_4. (b) Evolution of the real part of the capacitance vs. the frequency (above) and evolution of the imaginary part of the capacitance vs. the frequency (below).

To determine the real capacitance, the real and imaginary capacitance are plotted as a function of frequency (Figure 7.b), where:

$$C = C_{real} - j\, C_{imaginary}$$

$$C_{real}(\omega) = \frac{-Z_{imaginary}(\omega)}{\omega\left|Z(\omega)\right|^2}$$

$$C_{imaginary}(\omega) = \frac{-Z_{real}(\omega)}{\omega\left|Z(\omega)\right|^2}$$

In the plot, f_0 corresponds to $C_{real} = C_{LF}/2$; f_0 separates the capacitive behavior ($C_{real} > C_{LF}/2$) and the resistive behavior ($C_{real} < C_{LF}/2$) of the capacitor. f_0 corresponds to the maximum energy dissipation and $\tau_0 = 1/f_0$. Therefore Cd = 133 F/g which is in agreement on the capacitance measured by cyclic voltammetry.

The response at high frequencies show a deformed semicircle while the response at low frequencies does not show a line parallel to the y axis, suggesting that the system does not behave as a simple double layer capacitance. The deviation at low frequency usually shows the influence of mass transport, related to the microporous structure of the interface between electrode and electrolyte.[64]

Probe Beam Deflection

To evaluate the ion exchange coupled with the double layer charging, we use Probe Beam Deflection (PBD). The cyclic voltammetry (Figure 8. upper box) show a nearly constant current, typical of double layer charging. The PBD signal decreases at lower potential (E < 0.3 $V_{Ag/AgCl}$) and increases at higher potential. This is coherent with a double layer with a potential of minimum charge* of ca. 0.25-0.35 $V_{Ag/AgCl}$).

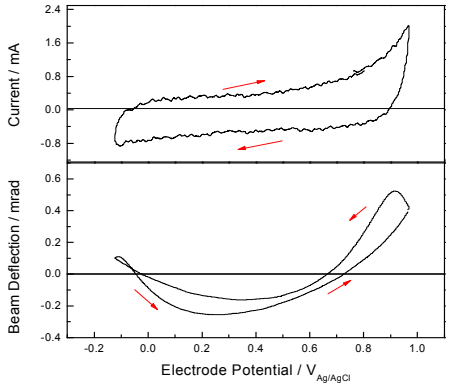

Fig. 8 Cyclic voltammetry (upper box) and cyclic deflectometry (lower box) of a HPC (400 nm) electrode in a 0.01 M KCl solution (scan rate 20 mV s^{-1}).

To evaluate the dynamic behavior, the PBD signal is monitored during time after the potential is switched between 0.0 and 0.9 $V_{Ag/AgCl}$ (Figure 9).

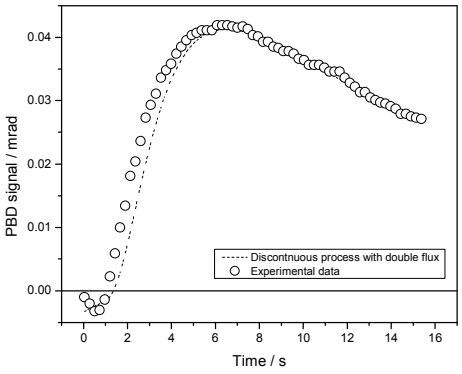

Fig.9 Chronodeflectometry of a dPC in 0.1 KCl. The potential is pulsed between 0 and 0.9 $V_{Ag/AgCl}$. The dashed line present the simulation using two discontinuous process of opposite sense.

Distance beam-electrode = 100 μm. $D_1 = 2.58\ 10^{-6}$ cm^2s^{-1}, $D_2 = 3\ 10^{-5}$ cm^2s^{-1}. $C_1 = 1\ 10^{-3}$ M. $C_2 = 1\ 10^{-4}$ M.

The double layer process should show only one ion exchanged (e.g. Cl^-):

$$C(-) + Cl^- \rightarrow C(+)Cl^- + n\ e^- \qquad (I)$$

where C(-) represents the carbon at potentials more negative than the potential of minimum charge (pmc) and C(+) represent the carbon at potentials more positive than the pmc. In that case, only one peak will be present.

It is noteworthy that the chronodeflectometry profile is fitted with a discontinuous process since the pore length in the hierarchical porous carbon is short enough to allow double layer charging in a negligible time compared with the span of the measurement (> 16 s).

However, a prepeak is observed in the chronodeflectometric signal. A possible explanation is the fact that, inside the pore is faster to dissociate water and adsorb OH^- instead of bringing Cl^- from the solution, because protons are faster ($D = 8.1\ 10^{-5}$ cm^2s^{-1}) than Cl^- ($D = 1.33\ 10^{-5}$ cm^2s^{-1}).[65] In that way, at short times, water is dissociated and OH^- is adsorbed, then H^+ are expelled creating a counterflux to the anion intake:

short time

$$C(-) + H_2O \rightarrow C(+)OH^- + H^+ + n\ e^- \qquad (II)$$

long time

$$C(-) + Cl^- \rightarrow C(+)Cl^- + n\ e^- \qquad (III)$$

$$C(+)OH^- + H^+ + Cl^- \rightarrow C(+)Cl^- + H_2O + n\ e^- \qquad (IV)$$

This is observed as a prepeak in the chronodeflectometry signal. Inside the pore, the local pH is higher than the bulk pH. At longer times, anions are inserted, OH^- ions are desorbed and protons are inserted making the internal pH equal to the external pH. Such local pH could affect the solution chemistry and/or electrochemistry of the analyte and should be taken into account when using porous electrodes.

The diffusion coefficients used for the fitting (Figure 9) correspond to the binary diffusion coefficient of KCl (main peak) and HCl (prepeak) since in a binary electrolyte like KCl, the electroneutrality maintenance links the mass transfer of anions and cations.[66]

sPC impregnation with PtRu

Previously, we have shown that catalytic metal nanoparticles (e.g. Pt) could be in-situ synthesized inside porous carbon by the formic acid method.[67]

With aim of testing the utility of HPC as support for the catalyst, a sample of dPC was loaded with 20 % (w/w) of Pt/Ru (1:1) as described in the experimental section. A transmission electron microscopy image of the PtRuNP-sPC (ESI. Figure S2) shows good nanoparticle dispersion, with nanoparticle size around 2 nm.

CO and Methanol electrooxidation on PtRuNP-sPC

The cyclic voltammogram in 1 M H_2SO_4 electrolyte (black dotted line in Figure 10) shows the characteristic features of carbon supported PtRu materials.[68]

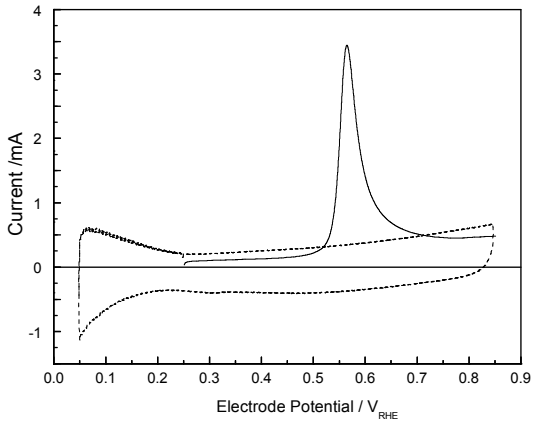

Fig. 10 CO stripping at 25ºC (dashed line) for PtRuNP-sPC. CV in clean electrolyte (dotted line). $E_{ad.}$= 0.25V, t_{ad} = 10 min. v = 20 mVs^{-1}

CO adsorption and stripping experiments were performed at 25 ºC. The adsorption was performed by exposition of the electrode to a CO saturated solution (0.92 mM)[69]) during 10 min, keeping the electrode potential fixed at 0.25 V. After that, clean electrolyte (CO free) was flushed for additional 20 min in presence of bubbling N_2, to prevent the presence of dissolved CO during the stripping. The CV shows a clear peak due to CO oxidation to CO_2.

$$CO + H_2O \rightarrow CO_2 + 2\ H^+ + 2e^- \qquad (V)$$

It is noteworthy that oxidation of CO adsorbed on Pt nanoparticles loaded inside a a monolithic porous carbon does not show the current due to CO oxidation.[67] However, simultaneous differential electrochemical mass (DEMS) spectroscopy measurements shows that CO_2 was being produced in the same potential range, indicating that CO was being oxidized (ESI, Figure S4). It seems that slow double layer charging, present in non hierarchical porous carbon, does not allow the distinction between charging and faradaic current during cyclic voltammetry experiments. Since DEMS only

detect volatile species, is insensitive to charging current effects and clearly show that CO electrochemical oxidation was occuring. In HPC electrodes, the open structure of the material diminishes the effect of slow charging and allows the CO oxidation current to be easily detected. From the CO adsorption and striping experiments, it is possible to measure an important parameter: the electrochemically active area of the metal nanoparticles. The CO oxidation charge in Figure 10 is 9.15 mC. Therefore, assuming 420 μCcm^{-2} for CO stripping, the electroactive surface area of the PtRuNO-sPC is 21.8 cm^2. Since the film contains 40 µg of nanoparticles, the calculation gives an area of 54.5 m^2g^{-1} for the surface area of the PtRu nanoparticles. The value is reasonable for small and highly distributed PtRu nanoparticles. The data show that PtRuNP-sPC is active to oxidize adsorbed redox species and cyclic voltammetry is able to distinguish between double layer charging and adsorbed species. The electrode is also able to oxidize methanol, (ESI, Figure S3) showing promise for electroanalysis of organic molecules which do not have reversible redox groups.

Oxygen reduction on CoOxNP-dPC

A possible way to to electrocatalyze oxygen reduction is to use redox catalysts, such as redox metal oxides.[70] Cobalt oxide nanoparticles were easily deposited inside dPC by cyclic voltammetry (as described in the experimental part). The electrode was tested for oxygen reduction (Figure 11).

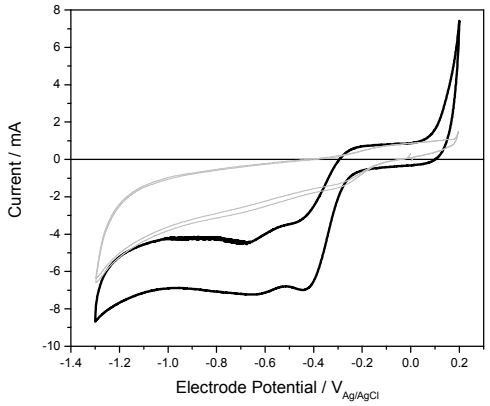

Fig.11 Cyclic voltammetry of a porous carbon modified with CoOx nanoparticles electrode in saturated O_2 solution (black line) and saturated with N_2 (grey line). Electrolyte = 0.1 M KOH, scan rate = 10 mVs^{-1})

The voltammogram of the modified electrode in oxygen saturated (0.24 mM [71]) basic (0.1 M KOH) solution (Figure 11) shows clearly two peaks due to the successive 2 electron transfer reactions occurring during oxygen reduction. By comparison, the elctrode show a featureless chaging current behaviousr in deareated (bubbling N_2 during 15 min) solution. The process at ca. -0.4 $V_{Ag/AgCl}$ involves the 1-electron reduction of oxygen which is mediated by quinone groups (Q) present at the carbon surface.[72]

$$Q + e^- \rightarrow Q^- \quad \text{(VI)}$$

$$Q^- + O_2 \rightarrow Q + O_2^- \quad \text{(VII)}$$

The $O_2^{\bullet-}$ ion disproportionate into O_2 and HO_2^- (VIII) or is reduced to HO_2^- (IX)

$$2\ O_2^{\bullet-} + H_2O \rightarrow HO_2^- + O_2 + OH^- \quad \text{(VIII)}$$

$$O_2^{\bullet-} + H_2O + e^- \rightarrow HO_2^- + OH^- \quad \text{(IX)}$$

The peroxide radical anion could also be produced by direct reduction at the carbon surface, but a slower rate.

The peroxide anion decompose into oxygen and OH^-

$$2\ HO_2^- \rightarrow O_2 + 2\ OH^- \quad \text{(X)}$$

Such reaction is catalyzed by redox hydroxides (like $Co(OH)_2$) which can be reversible converted into more oxidized species:

$$Co(OH)_2 + HO_2^- \rightarrow CoOOH + OH^- + H_2O \quad \text{(XI)}$$

to release O_2 by a coupled chemical reaction:

$$4\ CoOOH + 2\ H_2O \rightarrow 4\ Co(OH)_2 + O_2 \quad \text{(XII)}$$

or to be electrochemically reduced back to the hydroxide

$$CoOOH + e- + H_2O \rightarrow Co(OH)_2 + OH^- \quad \text{(XIII)}$$

The metal oxide nanoparticles have a large surface area where those reactions can occur. Its reduced size makes the electron transport inside the particle, towards the base carbon electrode, quite fast. Therfore, it is likely that reaction (XIII) dominates over (XII).

The peroxide anion is electrochemically reduced to hydroxide at ca. -0.62 $V_{Ag/AgCl}$

$$H_2O_2^- + e^- \rightarrow 2\ OH^- \quad \text{(XIV)}$$

Such reaction could also be catalyzed by cobalt oxide species. The results show that dPC modified with cobalt oxide nanoparticles are able to detect oxygen.

Arsenite oxidation on MeOx NP/dPC

Another relevant analyte is arsenic, a common contaminant of surface waters,[73,74] present as different ionic species. Metal oxides adsorb easily arsenic anions,[75] whose oxidation/reduction can be catalyzed by redox oxides. Hierarchical porous carbon, modified with in-situ produced cobalt oxide nanoparticles (CoOxNP-dPC) was used to detect arsenic ions in neutral solution (Figure 12). The cyclic voltammogram measured in the presence of As ions (full line) shows a clear oxidation peak which is not present in the CV measured in the absence of As ions (dashed line). The peak is likely due to the oxidation of As^{III} to As^{V} species, catalyzed by the cobalt oxide:

$$2\ Co(OH)_2 \rightarrow 2\ CoOOH + 2\ e^- \quad \text{(XV)}$$

$2\ CoOOH + AsO_3^{-3} + 2\ H_2O \rightarrow 2\ Co(OH)_2 + AsO_4^{-3} + 2\ OH^-$ (XVI)

It is likely that reaction (XVI) occurs with the anion adsorbed in the nanoparticle surface. The metal oxide nanoparticles have a large surface area where such adsorption can occur.

As it can be seen low levels (<200 ppm) of arsenic can be easily detected using cyclic voltammetry on modified HPC.

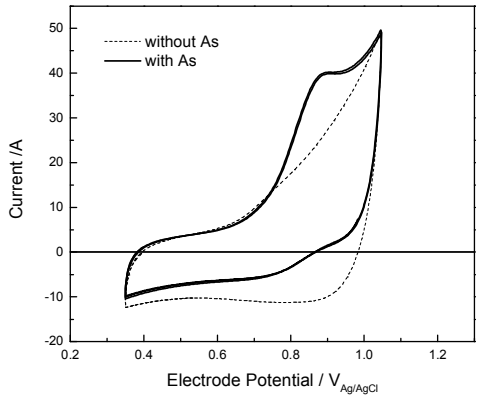

Fig. 12 Cyclic voltametry of a porous carbon electrode modified with CoOx nanoparticles in the absence (dashed line) and presence (full line) of AsO_3^{-3} (187.5 ppm) ions. Electrolyte = 0.1 M phosphate buffer (pH=7). Scan rate = 5 mVs^{-1}

Iron oxides can also be used to detect arsenic. In Figure 13 are shown the differential pulse volatmmograms of a dPC electrode modified with chemically produced magnetite (Fe_3O_4) nanoparticles (MagNP-dPC).

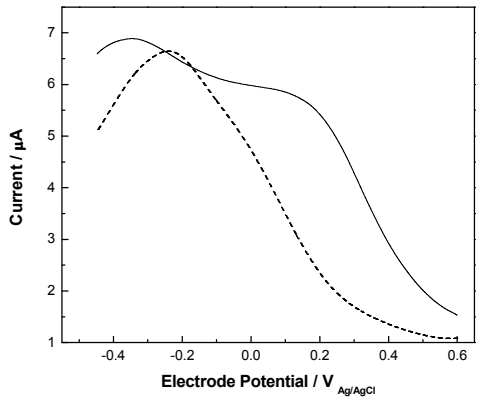

Fig. 13 Differential pulse voltammetry (DPV) of a dPC modified with Fe_3O_4 in the presence (full line) of $NaHAsO_3$ (300 ppm). The dashed line show the DPV of the electrode in absence of As. Scan rate = 20 mVs^{-1}. ΔE_{pulse}= 10 mV. t_{pulse}= 10 ms

The presence of the arsenite ions clearly change the DPV profile from a single peak (due to Fe^{II}/Fe^{III} redox couple) to two peaks, likely due to different iron oxide species with surface bonded arsenite. The mechanism is liekly similar to the one observed with cobalt hydroxide. The peaks are superimposed to a broad current background.

The data show that DPV could be used with HPC electrodes but the low definition of the peaks (against background current) suggest that charging effects are not completely eliminated by the pulse technique. This is likely to be related with slow double layer charging which makes that the charging current is still significative at the end of the potential pulse.

Oxygen reduction on PtMag-dPC

Oxygen is an interesting analyte in complex enviromental samples.[76] In those applications, high sensitivity to the analyte should be combined with low sensitivity to the matrix. Both platinum,[77] and FePt,[78] are effective electrocatalysts of oxygen reduction. We synthesize Pt decorated magnetite nanoparticles inside dPC by means of galvanic displacement of Fe_3O_4 nanoparticles with H_2Cl_6Pt. The presence of Pt on the particles was confirmed by the presence of proton reduction currents at potentials more cathodic than 0.0 V_{RHE} (ESI. Figure 5).

Then, we tested the reduction of oxygen on the material. As it can be seen (Figure 14) the peak due to inmobilized redox oxide (dashed line in Figure 14) shifted below the zero current axis due to the presence of a catalytic current for oxygen reduction. A likley catalytic mechanism involves the oxidation of Fe^{II} species by oxygen:

$3\ Fe(OH)_2 + O_2 = Fe_3O_4 + 3\ H_2O$ (XVII)

This reaction is catalyzed by the presence of Pt which allow breaking of the O_2 molecule.

The reduced species is regenerated by electrochemnical reduction of the magnetite nanoparticles :

$Fe_3O_4 + 2\ H^+ + 2\ e^- + 2\ H_2O = 3\ Fe(OH)_2$ (XVIII)

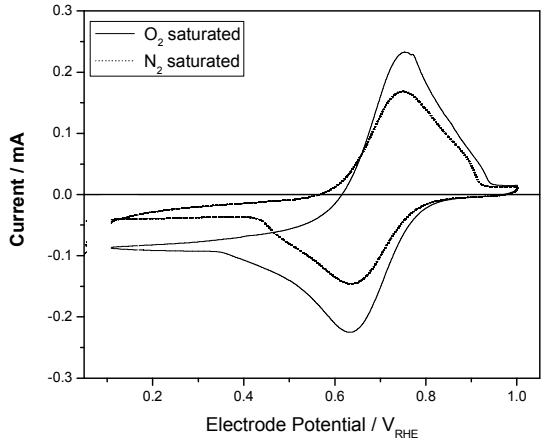

Fig.14 Oxygen (saturated solution) reduction on PtMagNP-dPC electrodes in the presence of 0.5 M methanol. Scan rate = 5 mVs^{-1}. Solution = 0.1 M H_2SO_4 solution saturated with O_2 (15 min bubbling gas).

The signal due to oxygen remains active in the presence of 0.5 M methanol (Figure 14), showing a good capacity of rejecting the interference. Rotating disk voltammetry measurements

show a current which increases with rotation rate, confirming the presence of mass transport controlled faradaic reactions.

Conclusions

Numerical calculations show that ideal large area electrodes could be used in electroanalysis disregarding the effect of charging currents. On the other hand, real porous electrodes could present slow double layer charging, compatible with a transmission line model (TLM), which could interfere with the faradaic measurements.

One way to produce porous electrodes with fast charging involves synthesizing hierarchical porous carbon (HPC) electrodes, where nanopores (micro and mesopores in IUPAC terminology) have short lengths due to the presence of macroporosity.

The synthesis of resorcinol-formaldehyde resins in the interstitial space of an opal made of silica nanoparticles allows to fabricate HPC. By removing the hard template before or after pyrolisis, it is possible to produce a double pore (sPC) or single pore carbon (dPC), respectively. SEM characterization of FIB prepared samples shows an open three dimensional structure. The specific double layer capacitance (measured by cyclic voltammetry and AC impedance) is in the order of 130 Fg^{-1}, suggesting that the material has a large (ca. 650 m^2g^{-1}) specific surface. Chronoamperometric measurements of monolithic porous carbon (without macropores) shows slow double layer charging compatible with a semi-infinite TLM. On the other hand, both dPC and sPC show a finite TLM, making them less affected by charging current effects.

Chronodeflectometric measurements of dPC in neutral media a show a defined pre-peak which seems related with an increase of local pH (inside the pore) due to restricted diffusion of ions.

Both sPC and dPC were modified by in-situ (chemical or electrochemical) synthesis of metal or metal oxide nanoparticles. sPC modified with PtRu nanoparticles is able to efficiently oxidize CO and methanol. CO monolayer oxidation current was easily detected unlike previous results with modified non hierachical porous carbon.[67]

dPC electrodes modified with electrochemically grown cobalt oxide nanoparticles seem able to detect molecular oxygen or arsenic ions.

dPC modified with magnetite nanoparticles, chemically grown inside the carbon, could be used to detect arsenite by differential pulse voltammetry. dPC modified with magnetite nanoparticles decorated with Pt, by galvanic displacement reaction, show clear signal for oxygen reduction even in the presence of 0.5 M methanol.

Hierarchical porous carbon, modified with electrocatalytic nanoparticles, seems to be a promising material for electroanalysis.

Acknowledgements

R.C.R y A.B.M. thank CONICET and FONCYT (respectively) for graduate fellowships. D.F.A., G.A.P. y C.A.B. are permanent research fellows of CONICET. Funding by FONCYT, CONICET, MinCyT (Cordoba) and SECYT-UNRC is gratefully acknowledged. F. Soldera and F. Mucklich are thanked for the FIB-SEM measurements.

Notes and references

[a] Chemistry Department, National University of Rio Cuarto (UNRC), 5800-Rio Cuarto, ARGENTINA. FAX: +543584676233; Tel: +543584676233; E-mail:cbarbero@exa.unrc.edu.ar

† Electronic Supplementary Information (ESI) available: SEM of SiO_2 opal, HRTEM of PrRuNP-sPC, CV of methanol on PtRuNP-sPC, CV and DEMS of adsorbed CO on Pt nanoparticles deposited inside non hierachical porous carbon, CV of PtMagNP-dPC to detect proton reduction. See DOI: 10.1039/b000000x/

‡ * The potential of minimum charge (pmc) is the potential where a balance exists between negative and positive charges. It is the polycrystalline equivalent of the potential of zero charge (pzc) which is valid for single crystals.

References

1 R.L. McCreery, Carbon Electrodes: Structural Effects on Electron Transfer Kinetics, in *Electroanalytical Chemistry*, A.J. Bard (Ed.), Dekker, NY, 1991, Vol. 17, pp. 221-374.
2 M.Marti Villalba, J. Davis, *J Solid State Electrochem*, 2008,**12**, 1245
3 E. Majid, S. Hrapovic, Y. Liu, K.B. Male, J.H.T. Luong, *Anal. Chem.*, 2006, **78**, 762
4 I.S. Vancara, K. Vytras, K. Kalcher, A. Walcarius, J. Wang, *Electroanalysis*, 2009, **21**, 7
5 G.A. Rivas, M.D. Rubianes, M.C. Rodrıguez, N.F. Ferreyra, G.L. Luque, M.L. Pedano, S.A. Miscoria, C. Parra, *Talanta*, 2007, **74**, 291.
6 Y. Shao, J. Wang, H. Wu, J. Liu, I. A. Aksay, Y. Lin, *Electroanalysis*, 2010, **22**, 1027
7 A. Walcarius, *Trends in Analytical Chemistry*, 2012, **38**, 79
8 M.M. Bruno, N.G. Cotella, M.C. Miras, T. Koch, S. Seidler, C. Barbero, *Coll. Surf. A: Phys. Eng.*,, 2010, **358**, 13
9 M.M. Bruno, N.G. Cotella, M.C. Miras, C.A. Barbero, *Coll. Surf. A: Phys. Eng.*, 2010, **362**, 28
10 Y. Deng, C. Liu, T. Yu, F. Liu, F. Zhang, Y. Wan, L. Zhang, C. Wang, B. Tu, P.A. Webley, H. Wang, D. Zhao, *Chem. Mater.*, 2007, **19**, 3271.
11 Z. Wang, F. Li, N.S. Ergang, A. Stein, *Chem. Mater.* 2006, **18,** 5543.
12 B. Sakintuna, Y. Yürüm, *Ind. Eng. Chem. Res., 2005,* **44**, 2893.
13 M.M. Bruno, N.G. Cotella, M.C. Miras, C.A. Barbero, *Chem. Commun.,* 2005, 5896.
14 G. Wang, L. Zhang, J. Zhang, *Chem. Soc. Rev.,* 2012,**41**, 797.
15 J. Balach, M.M. Bruno, N.G. Cotella, D.F. Acevedo, C.A. Barbero, *J. Power Sources.*, 2012, **199**, 386.
16 A.F. Gross, A.P. Nowak, *Langmuir,* 2010, **26**, 11378.
17 O.D. Vele, A.M. Lenhoff, *Curr. Opin. Colloid. In.* 2000, **5**, 56.
18 F. Ruo-wen, L. Zheng-hui, L. Ye-ru, L. Feng, X. Fei, W. Ding-cai, *New Carbon Mater.* 2011, **26,** 171.
19 A.M. Baena-Moncada, G.A. Planes, M.S. Moreno, C.A. Barbero, *J. Power Sources*, 2013, **221**, 42.
20 E. Frackowiak, F. Beguin, *Carbon,* 2001, **39**, 937.
21 B.E. Conway. *Electrochemical Supercapacitors: Scientific Fundamentals and Technological Applications*. Springer, Berlin, 1999.
22 G. Lang, C.A. Barbero, *Laser Techniques for the Study of Electrode Processes*, Springer, Berlin, 2012
23 C.A. Barbero, *Phys. Chem. Chem. Phys*., 2005, **7**, 1885.
24 G. García, M.M. Bruno, G.A. Planes, J.L. Rodriguez, C. Barbero, E. Pastor, *Phys. Chem. Chem. Phys*., 2008, **10**, 6677.
25 G.A. Planes, M.C. Miras, C.A. Barbero, *Chem. Commun.,* 2005, 2146.

26 E.L. Principe, High-density FIB-SEM 3D nanotomography: with applications of real-time imaging during FIB milling in *Focused Ion Beam Systems. Basics and Applications*, N.Yao, Ed. Cambridge University Press, Cambridge, 2007.

27 J Balach, F Miguel, F Soldera, DF Acevedo, F Mücklich, CA Barbero, *J Microsc*., 2012, **246**, 274,

28C.M. Welch, R.G. Compton, *Anal. Bioanal. Chem*., 2006, **384**, 601

29 A.S. Aricò, S. Srinivasan, V. Antonucci, *Fuel Cells,* 2001, **1**, 133.

30 A. Habrioux, E. Sibert, K. Servat, W. Vogel, K. B. Kokoh, N. Alonso-Vante, *J. Phys. Chem. B*, 2007, **111,** 10329.

31 G. García, J.A. Silva-Chong, O. Guillén-Villafuerte, J.L. Rodríguez, E.R. González, E. Pastor, *Catal. Today*, 2006, **116,** 415.

32 C.E. Lee, S.H. Bergens, *J. Phys. Chem. B*., 1998, **102**, 193.

33 H.A. Gasteiger, N. Markovic, P.N. Ross Jr., E. Cairns, *J. Phys. Chem*., 1994, **98**, 617.

34 G.A. Planes, G. García, E. Pastor*, Electrochem. Commun*., 2007, **9**, 839.

35 Z. Chen, D. Higgins, A. Yu, L. Zhang, J. Zhang, *Energy Environ. Sci.,* 2011,**4**, 3167

36 L. Trotochaud, J.K. Ranney, K.N. Williams, S.W. Boettcher, *J. Am. Chem. Soc.*, 2012, **134**, 17253.

37 U. Yogeswaran, S-M. Chen, S-H. Li, *Electroanalysis*, 2008, **20**, 2324.

38 C. Barbero, G.A. Planes, M.C. Miras, *Electrochem. Commun*., 2001, **3** , 113.

39 A. Salimi, R. Hallaj, S. Soltanian, H. Mamkhezri, *Anal. Chim. Acta* 2007, **594**, 24.

40 A. Salimi, H. Mamkhezria, R.Hallaj, S. Soltanian, *Sens. Actuat. B,* 2008, **129**, 246.

41 L.H. Reddy, J. L. Arias, J. Nicolas, P. Couvreur, *Chem. Rev.*, 2012, **112**, 5818

42 C-L. Lee, C-M. Tseng, *J. Phys. Chem.* C, 2008, **112,** 13342.

43 W. Wang, B. Gu, L. Liang, W. Hamilton, *J. Phys. Chem. B*., 2003, **107,** 3400.

44 G. M. Jenkins, K. Kawamura, *Polymeric Carbons: Carbon Fibre, Glass and Char*, Cambridge University Press, Cambridge, 2011.

45 W. H. Lizcano-Valbuena, V. A. Paganin, E. R. González, *Electrochim. Acta*. 2002, **47**,3715

46 M. Mikhaylova, D.K. Kim, N. Bobrysheva, M. Osmolowsky, V. Semenov, T. Tsakalakos, M. Muhammed*, Langmuir,* 2004, **20,** 2472.

47 J. Zhang , Y. Mo , M. B. Vukmirovic , R. Klie , K. Sasaki , and R. R. Adzic, *J. Phys. Chem. B*, 2004, **108**, 10955.

48 A. Velichko, C. Holzapfel, F. Mücklich, *Advanced Engineering Materials*, 2007, **9**, 39–45.

49 B. Fang, J.H. Kim, M. Kim, J.-S. Yu, *Chem. Mater*., 2009, **21**, 789.

50 E. Frackowiak, F. Béguin, *Carbon,* 2001, **39**, 937.

51 W. Xing, S.Z. Qiao, R.G. Ding, F. Li , G.Q. Lu, Z.F. Yan, H.M. Cheng, *Carbon.*, 2006, **44**, 216.

52 L.Shen, C. Yuan, H. Luo, X. Zhang, K. Xu, F. Zhang, *J. Mater. Chem.* 2011, **21**, 761.

53 Y. Wu, Z. Wen, J. Li, *Adv. Mate*r. 2011, **23**, 1126.

54 F. Garay, C. Barbero, *Anal. Chem*., 2006, **78**, 6740-6746.

55 A.J. Bard, L.R. Faulkner, *Electrochemical Methods: Fundamentals and Applications*, Wiley; New York, 2000.

56 Samuel P. Kounaves, Voltammetric Techniques in *Handbook of Instrumental Techniques for Analytical Chemistry*, Frank A. Settle, Ed., Prentice Hall PTR, New York, 1997.

57 R. de Levie, *Electrochim. Acta*, 1964, **9**, 1231.

58 X. Jin, L. Zhuang, J. Lu, *J. Electroanal. Chem*., 2001, **519**, 137.

59 R.W. Pekala, *J. Mater. Sci*., 1989, **24**, 3221.

60 R.W. Pekala, C.T. Alviso, J.D. LeMay, *J. Non-Crys. Sol.*, 1990, **125**, 67.

61 F. Lufrano, P. Staiti, Int. *J. Electrochem. Sci*. 2010, **5**, 903.

62 X. Zhao, H. Tian, M. Zhu, K. Tian, J.J. Wang, F. Kang, R.A. Outlaw. *J. Power Sources*., 2009, **194**, 1208.

63 J. R. Macdonald, *Ann. Biomed. Eng.*, 1992, **20**, 289.

64 M.G. Sullivan, B. Schnyder, M. Bärtsch, D. Alliata, C. Barbero, R. Imhof, R. Kötz, *J. Electrochem. Soc.,* 2000*,* **147**, 2636.

65 C.A. Wraight, *Biochim. Biophy. Acta,* 2006, **1757**, 886.

66 F. Garay, C.A. Barbero, *Anal. Chem*. 2006, **78**, 6733.

67 M.M. Bruno, G.A. Planes, M.C. Miras, C.A. Barbero, E. Pastor Tejera, J.L. Rodriguez, *Mol. Cryst. Liq. Cryst.,* 2010, **521**, 229.

68 J.R.C. Salgado, F. Alcaide, G. Álvarez, L. Calvillo, M.J. Lázaro, E. Pastor, *J. Power Sources*. 2010, **195**, 4022

69 D.A. Wiesenburg, N.L. Guinasso, *J.Chem. Eng. Data,* 1979, **24**, 356.

70 Y. Wang, D. Zhang, H. Liu, *J. Power Sources,* 2010, **195**, 3135.

71 J. Emsley, Oxygen in *Nature's Building Blocks: An A-Z Guide to the Elements.* Oxford University Press. Oxford, 2001.

72 J. Xu, W.H. Huang, R.L. McGreery, *J. Electroanal. Chem*., 1996, **410**, 235; T. Ohsaka, L.Q. Mao, K. Arihara, T. Sotomura, *Electrochem.Commun.* 2004, **6**, 273; K. Vaik, D.J. Schiffrin, K. Tammeveski, *Electrochem. Commun*. 2004, **6**, 1; K. Tammeveski, K. Kontturi, R.J. Nichols, R.J. Potter, D.J. Schiffrin, *J. Electroanal. Chem*., 2001,**515**,101.

73 K. Mandal, K. T. Suzuki, *Talanta* 2002, **58**, 201.

74 A. Davis, D. Sherwin, R. Ditmars, K. A. Hoenke, *Environ. Sci. Technol.* 2001, **35**, 2401.

75 S.R. Chowdhury, E.K. Yanful, *Water Env. J.l*, 2011, **25**, 429.

76 F.X. Simon, Y. Penru, A.R. Guastalli, J. Llorens, S. Baig, *Talanta*, 2011, **85**, 527.

77 I.E.L. Stephens, A.S. Bondarenko, U. Grønbjerg, J. Rossmeis, I. Chorkendorff, *Energy Environ. Sci*., 2012,**5**, 6744.

78 C. Song, J. Zhang in *PEM Fuel Cell Electrocatalyst and Catalyst Layer. Fundamentals and Applications*. J. Zhang, Ed., Springer, Berlin, 2008.

Electronic supplementary information of FD164

Electroanalysis using modified hierarchical nanoporous carbon materials

Rusbel Coneo Rodriguez, Angelica Baena Moncada, Diego F. Acevedo, Gabriel A. Planes, Maria C. Miras and Cesar A. Barbero

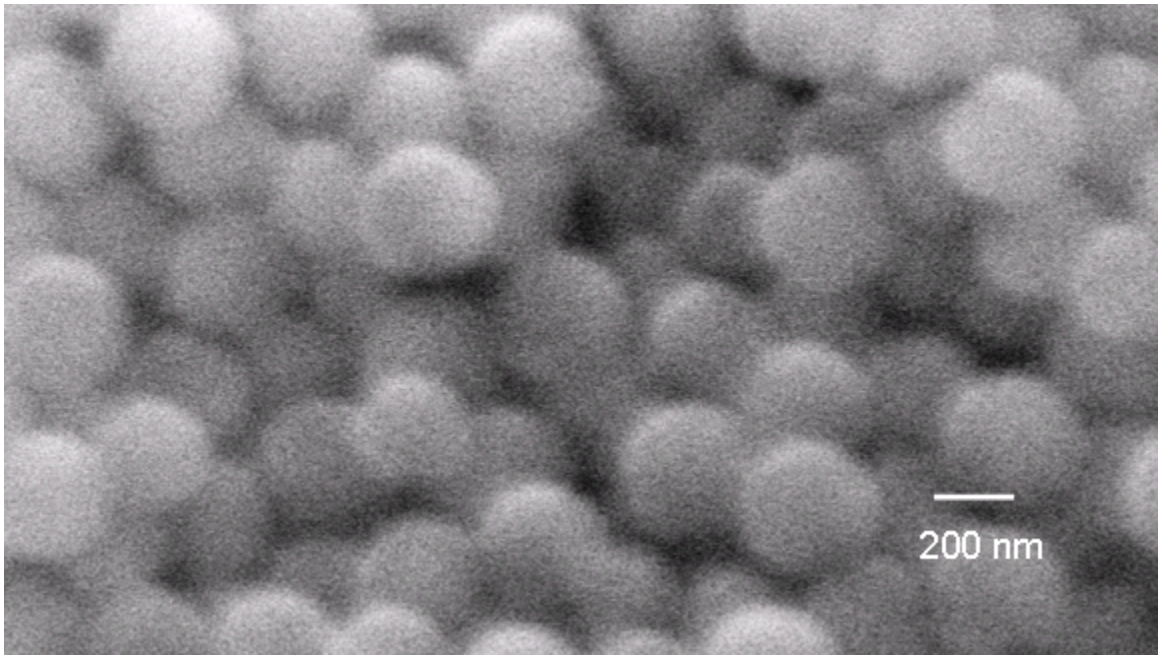

Figure S1
Scanning electron microscopy of an opal formed by SiO_2 nanopartucles.

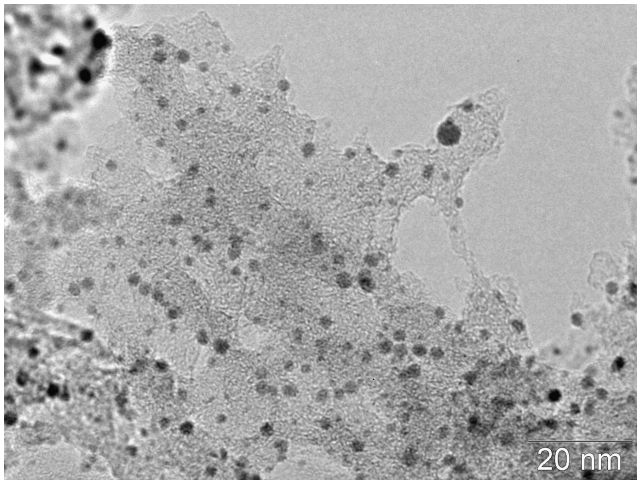

Figure S2
High resolution microscopy of a sPC with PtRu nanoparticles

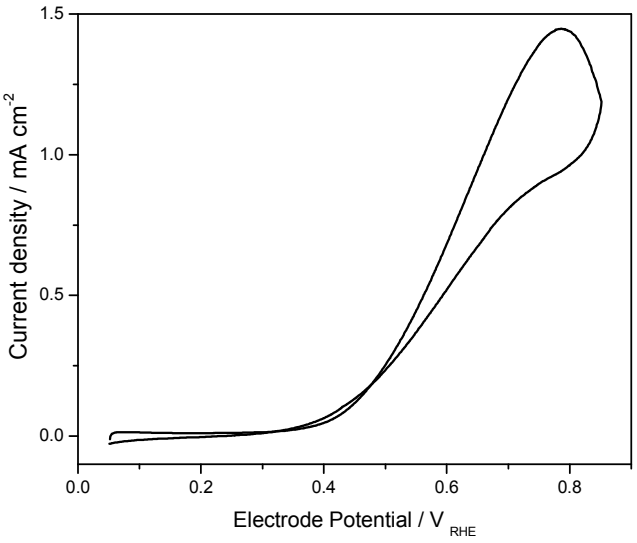

Figure S3.

CV at 60 ºC in 1 M CH_3OH / 1 M H_2SO_4 for PtRuNP-sPC . v = 20 mVs^{-1}

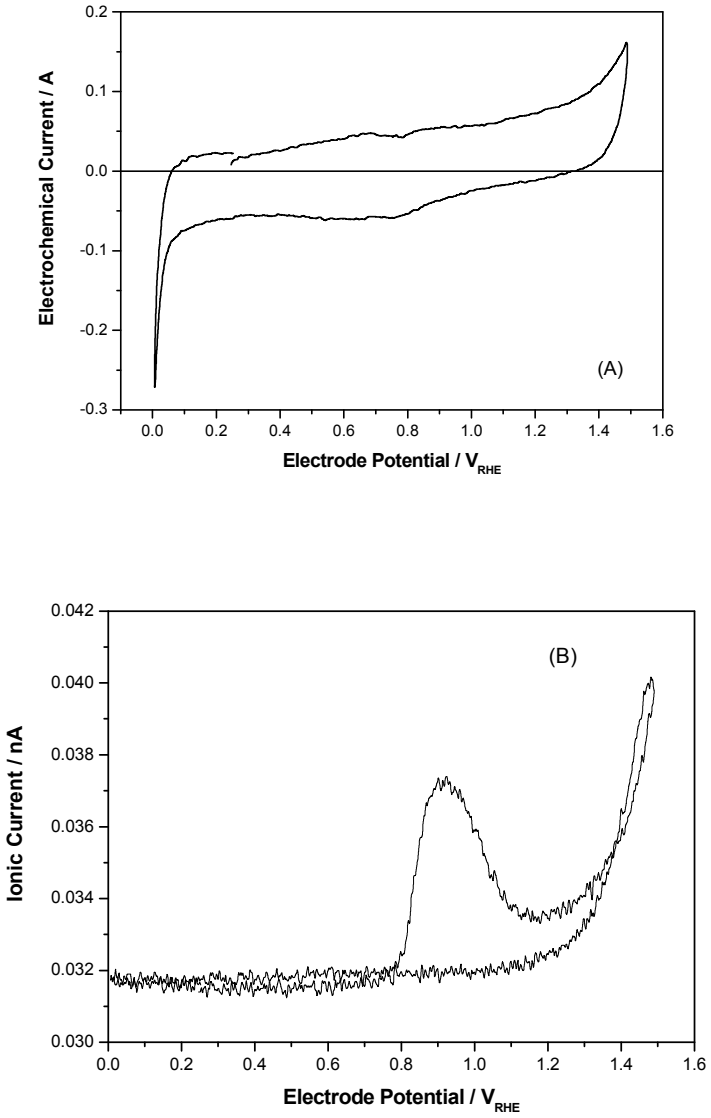

Figure S4.
(A) cyclic voltammogram and (B) DEMS signal of adsorbed CO on a porous vitreous carbon electrode loaded with Pt nanoparticles. Electrolyte = 0.5 M H_2SO_4. Scan rate = 1 mV/s

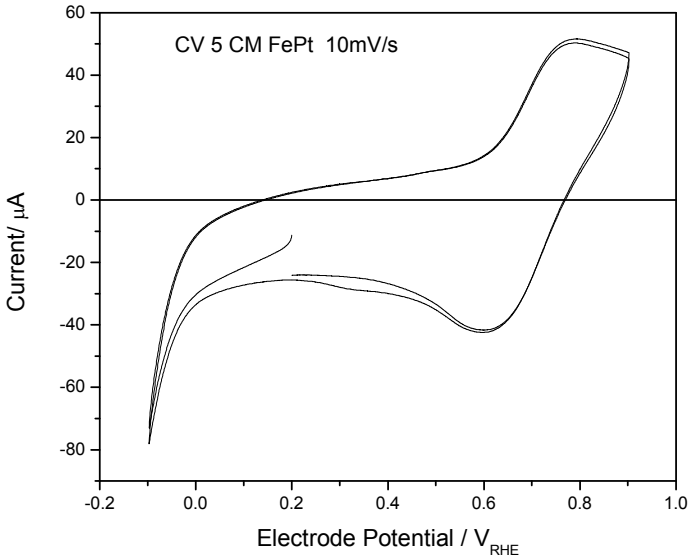

Figure S5.
Cyclic voltammogram of a dPC electrode loaded with Pt decorated magnetite nanoparticles in deareated 0.5 M H_2SO_4.